

L I C E N C E T O M C M A S T E R U N I V E R S I T Y

This THESIS has been written
[Thesis, Project Report, etc.]

by DOLORES DURANT for
[Full Name(s)]

Undergraduate course number 4K6 at McMaster
University under the supervision/direction of
 Dr. Paul M. Clifford .

In the interest of furthering teaching and research, I/we
hereby grant to McMaster University:

1. The ownership of 3 copy(ies) of this
work;
2. A non-exclusive licence to make copies of
this work, (or any part thereof) the
copyright of which is vested in me/us, for
the full term of the copyright, or for so
long as may be legally permitted. Such
copies shall only be made in response to a
written request from the Library or any
University or similar institution.

I/we further acknowledge that this work (or a surrogate
copy thereof) may be consulted without restriction by any
interested person.

Signature of Witness,
Supervisor

Signature of Student

 13 Jun 89
date

EVOLUTIONARY ASPECTS
OF
HUERFANO BUTTE
COLORADO

EVOLUTIONARY ASPECTS

OF

HUERFANO BUTTE

COLORADO

by

DOLORES G. DURANT

A Thesis

Submitted to the Department of Geology
in Partial Fulfilment of the Requirements
for the Degree

Honours Bachelor of Science

McMaster University

April, 1989

BACHELOR OF SCIENCE (1989)
(Geology)

McMaster University
Hamilton, Ont.

TITLE: EVOLUTIONARY ASPECTS OF HUERFANO BUTTE COLORADO

AUTHOR: Dolores G. Durant

SUPERVISOR: Dr. Paul Clifford

NUMBER OF PAGES: viii, 53

SCOPE AND CONTENTS:

Gabbroic dyke and syenitic plug intrusives have been sampled and studied across Huerfano Butte.

Petrography and geochemical analyses were performed on selected specimens; from these analyses chemical variation diagrams have been prepared. Crystal Size Distribution analyses have been done on magnetites and olivines to determine crystal nucleation and growth rate in the dyke. These data have been used to infer aspects of the evolution of Huerfano Butte.

ACKNOWLEDGEMENTS

The writer would like to express her deepest appreciation to Dr. Paul M. Clifford who suggested the thesis topic and continually offered his time and assistance during the length of the project.

The writer also wishes to thank Dr. Burley in regard to discussion pertaining to the identification of various minerals.

Many thanks are also extended to Jack Whorwood for his photographic expertise; to Len Zwicker for the thin section preparation; to Marilyn Gris for the use of her new computer; to Brad Gris for the preparation of many graphs for the CSD analyses; and to all the others who have helped in any way.

TABLE OF CONTENTS

Acknowledgements	iii
Table of Contents	iv
List of Figures	v
List of Plates	vi
List of Tables	vii
Abstract	viii
1.0 General Setting	
1.1 Geographical Location	1
1.2 Geological Setting	1
2.0 Petrography	10
3.0 Geochemistry	
3.1 Introduction	16
3.2 Chemical Trends	16
3.3 Interpretation	30
3.4 Comparisons	31
4.0 Crystal Size Distribution Theory	
4.1 Introduction	36
4.2 Outline of CSD Theory	37
4.3 Methodology of CSD Analysis	37
4.4 Results	41
4.5 Interpretation	45
4.6 Error Discussion	49
4.7 Conclusions	50
Bibliography	51

LIST OF FIGURES

1.1 Location of Huerfano Butte	2
1.2 Precambrian fault trends	4
1.3 Late Paleozoic highlands	5
1.4 Laramide uplifts	6
1.5 Subduction of Farallon plate	8
3.1 Harker diagrams MgO, Fe ₂ O ₃ , CaO	23
3.2 Harker diagrams Al ₂ O ₃ , Na ₂ O, K ₂ O	24
3.3 Nomenclature classification	25
3.4 AFM diagram	27
3.5 REE - gabbroic dyke	28
3.6 REE - syenitic plug	29
3.7 Nb vs. Zr comparison	33
3.8 REE comparison	34
3.9 Alkali and lime trends	35
4.1 CSD curve for magnetite	44
4.2 CSD curve for olivine	44
4.3 Theoretical CSD curve for annealing	48

LIST OF PLATES

1. Magnification of thin section

12

LIST OF TABLES

2.1 Mineral Modal Percentages	14
3.1 Major element oxide concentrations	17
3.2 Major element oxides normalized to 100%	18
3.3 CIPW norms	19
3.4 Trace elements; X-ray Fluorescence	20
3.5 Trace elements; Neutron Activation	21
4.1 Magnetite grain measurements	42
4.2 Olivine grain measurements	43
4.3 CSD values for magnetite	46

ABSTRACT

Huerfano Butte, one of a host of igneous bodies associated with the Rio Grande Rift, is a syenitic plug cut by a gabbroic dyke. Both mineralogy and chemistry imply that the syenite represents a fractionated derivative from a gabbroic source. This conclusion in turn suggests either that the syenite was extracted from the top of a magma reservoir, with the dyke representing the lower level of that reservoir; or that two local separate sources were involved. REE chondrite - normalized enrichment patterns suggest that plagioclase was significantly fractionated in the production of the syenite. Crystal Size Distribution (CSD) analysis carried out on magnetites show a linear correlation between $\ln n$ (number crystals per size class) versus size class. This suggests continuous nucleation and growth; also nucleation densities and growth rates are about one order of magnitude less than those for Makaopuhi lava lake, and comparable with a lesser degree of undercooling at Huerfano Butte. CSD analysis of olivines yields a convex upward distribution curve, implying non-continuous growth, and augmentation of larger grains by resorption of smaller grains.

1.0 GENERAL SETTING

1.1 Geographical Location

Huerfano Butte is located at longitude $37^{\circ}46'05''$ N and latitude $104^{\circ}48'50''$ S in the state of Colorado in the western United States (Fig. 1.1). It is situated in the south central part of the state on the Great Plains just east of the Sangre de Cristo Range of the South Rocky Mountains. It is an isolated cone shaped butte roughly 180 meters in diameter approximately 16 kilometers north of Walsenburg on Interstate 25.

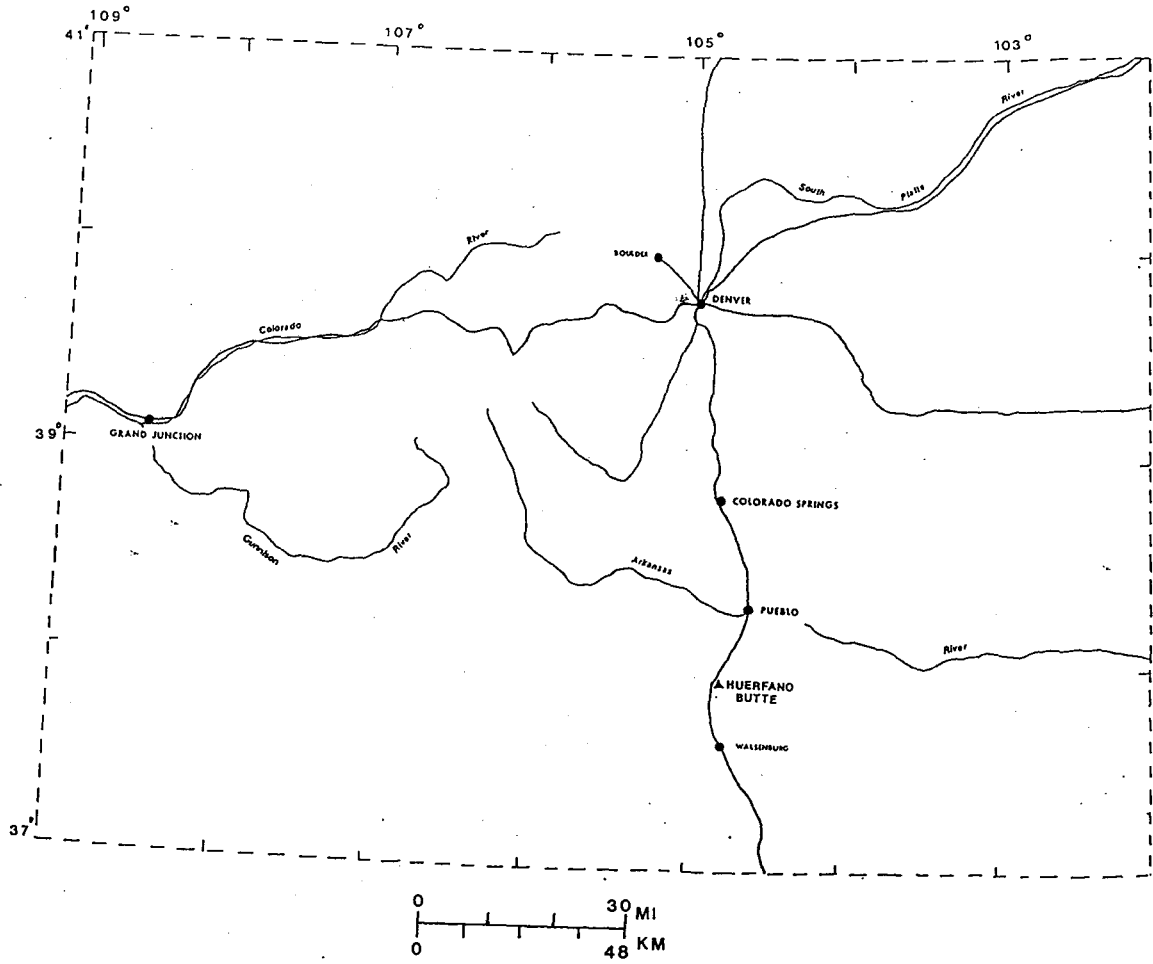
1.2 Geological Setting

The local geology of south central Colorado is dominated to the east by the Great Plains Stable Craton and to the west by zones which have been sites of repeated orogeny.

The cumulative effect of several periods of orogeny, uplift, and erosion are seen in the present day Rocky Mountains.

At least three periods of Precambrian deformation occurred creating an extensive network of major faults

**Fig. 1.1 Map of the state of Colorado showing location
of Huerfano Butte.**



and fault systems (Fig. 1.2) in a mainly north-northwest trend (Tweto, 1980a).

The Late Paleozoic was also a time of extensive tectonism with much reactivation of old faults resulting in at least three large highlands (Fig. 1.3); the Apishapa, Front Range, and Uncompahgre-San Luis Highlands that reinforced the north-northwest grain (Tweto, 1980b).

Another major period of tectonism occurred with the Laramide beginning in the Late Cretaceous. Deformational effects were constrained by the existing north-northwest fault system. There was uplift of many new mountain ranges along with subsidence that produced many new basins adjacent to faults that had been reactivated (Fig. 1.4). This same period also saw igneous activity in the form of volcanism and intrusions. The abundance of volcanic detritus seen in sedimentary rocks from this period suggests that volcanic edifices topped many of the intrusions and that they have subsequently eroded away (Tweto, 1980c).

Between 32 and 27 M.y. ago, a regime of regional extension began that again reactivated old faults causing rifting, volcanism, and intrusions that resulted in the Rio Grande Rift system (Chapin, 1979). The cause of this broad extension may have been due to the subduction of

Fig. 1.2 Location of major Precambrian fault trends
(after Tweto, 1980a).

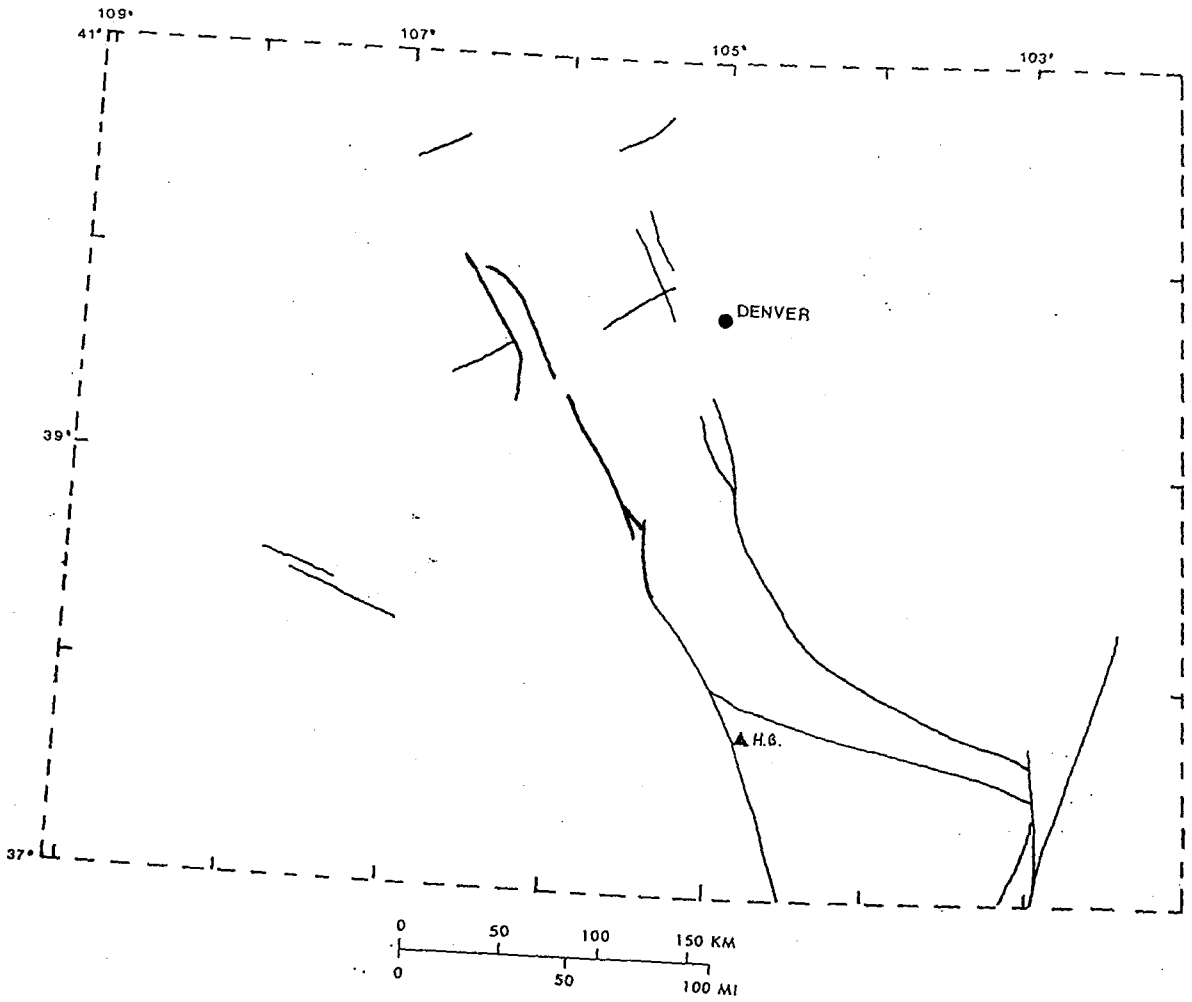


Fig. 1.3 Location of Late Paleozoic highlands (modified from Tweto, 1980b) .

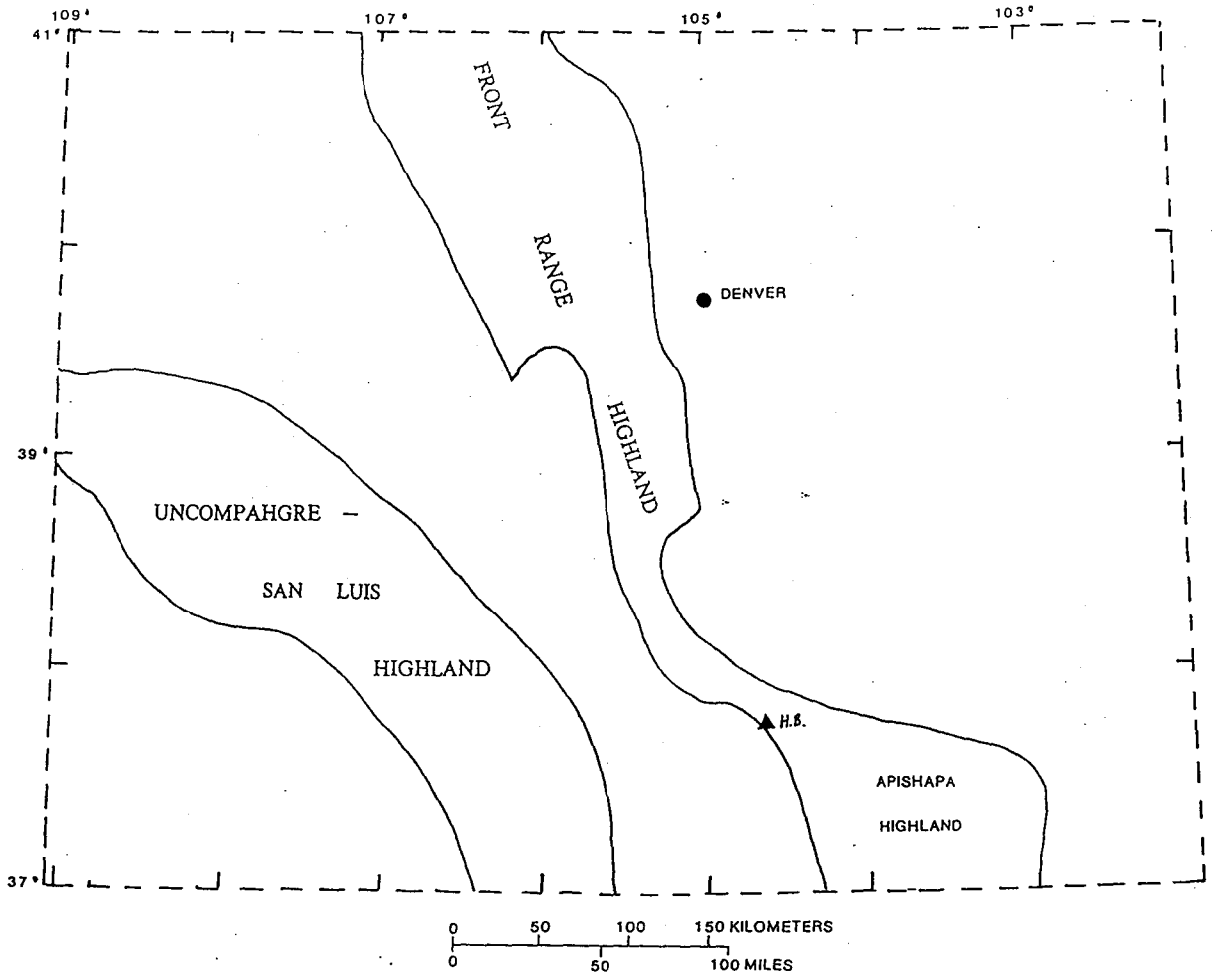
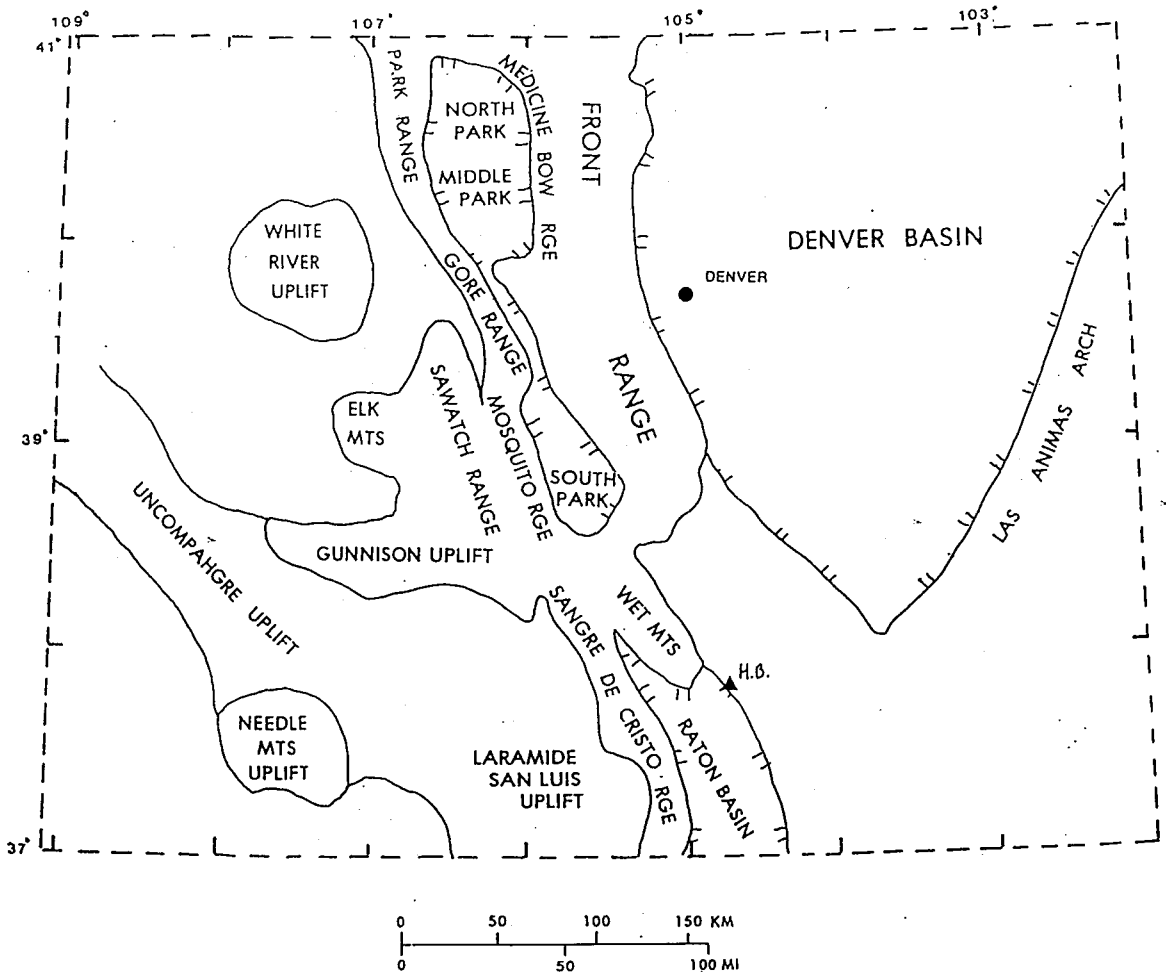


Fig. 1.4 Location of major Laramide features (modified from Tweto, 1980c).

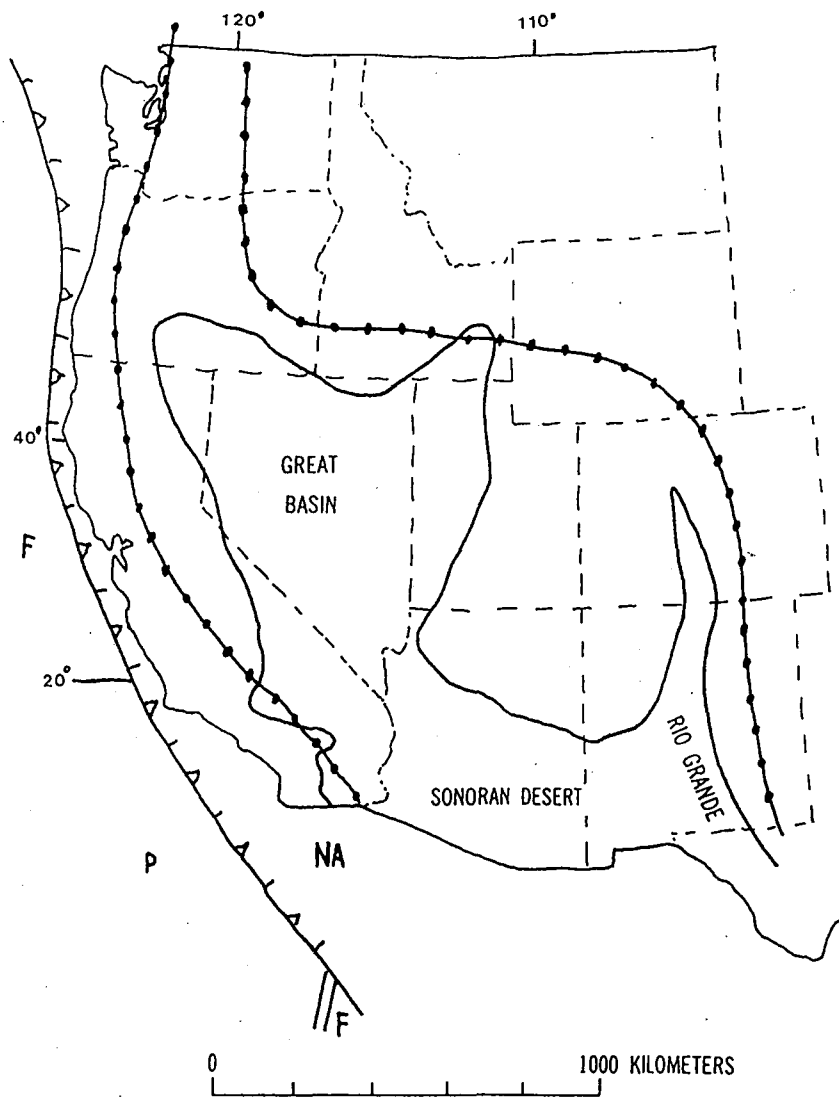


the Farallon plate by the North American plate. The resulting volcanic arc extended far inland (Fig. 1.5) due to the rapid rate of convergence between the two plates causing a low angle of subduction (Eaton, 1979).

During the period of 30 to 20 M.y., the Rio Grande Rift was generally characterized by rapid spreading, eruption of basaltic andesites and fault block rotation. All these indicate that the area was undergoing intra-arc extension. Igneous activity signalled the beginning of rifting with the production of voluminous basalts and a change from intermediate to bimodal silicic and mafic composition. The oldest flows directly attributable to the Rio Grande Rift are 26 to 27 M.y. old (Tweto, 1979).

One of the more spectacular examples of such rift-related volcanic activity is the large dyke system and intrusive centres of the Spanish Peaks complex. This has been dated at 22 to 27 M.y. (Stormer, 1972) and 19 to 25 M.y. (Marvin et al, 1974, fide Tweto, 1979). Thus it is probably related to the rifting even though actual placement pattern was probably controlled by crustal stresses from earlier orogenies (Johnson, 1970). Rocks of the complex are mainly syenodiorite but range from gabbroic to granitic (Johnson, 1968). The average intermediate composition of these rocks differs from

Fig. 1.5 Subduction of Farallon plate and resulting volcanic arc between 30 and 20 M.y. (modified from Eaton, 1979)



strictly rift-related compositions and implies a cratonic environment along the border of the rift. Thus rifting is probably not directly responsible for their origin but is probably their ultimate "raison d'etre" (Tweto, 1979).

In the vicinity of the Peaks, there are several enigmatic isolated plugs, locally termed Buttes. Huerfano Butte is one of these plugs. It is very close to the Spanish Peaks stocks and has been dated at 25 M.y. by Stormer (1972). Its composition is gabbroic to syenitic and would seem to have common origins with the Spanish Peaks system if not strictly part of it. Huerfano Butte seems to be a plug with a dyke in the centre. It does not seem to be part of the Spanish Peaks dyke system as there is no visible dyke-like feeder pointing towards the Spanish Peaks. Thus there seems to be no obvious direct stress control on the emplacement of Huerfano Butte unlike the controls hypothesized for the Spanish Peaks dykes.

2.0 PETROGRAPHY

Inspection of hand specimens of the rocks of Huerfano Butte reveals the presence of both mafic and felsic rocks. The mafic specimens are medium gray and medium grained with visible phenocrysts of biotite, olivine, and augite. These rocks are found at the centre of Huerfano Butte. The felsic specimens are buff coloured and coarse grained with visible phenocrysts of biotite and feldspars.

Two thin sections of the mafic specimens were examined. The essential minerals are olivine, augite, biotite, and feldspars. Accessory minerals include opaques, apatite, sphene, and minor serpentine and magnetite resulting from limited alteration of olivine.

Augite is the most abundant phenocryst phase. The crystals are subhedral to anhedral and pale green in colour. Continuous crystal zoning often occurs in the larger grains probably as a gradual change from augite interiors to aegirine-augite rims. Smaller grains often occur in clusters and are often found surrounding larger grains.

Another phenocrystic mineral, biotite, is seen as plates. It is very pleochroic, from pale brown to deep red, probably indicating Ti substitution.

Olivine is present as well, up to 5 mm in length. It is subhedral to anhedral with characteristic curved fractures lined with small amounts of the alteration products serpentine and magnetite.

Plagioclase is the most abundant phase in the groundmass and makes up about 29% of the rock. It ranges in composition from about An40 to An60 including both andesine and labradorite, probably in about equal proportions. The crystals are subhedral laths and often show both albite and Carlsbad twinning. Some crystals have a wavy birefringence that could be due to stress deformation as it attempted to make space to grow or it could be a compositional zoning of high temperature calcic cores to low temperature more sodic rims.

Sanidine is also present interspersed with the plagioclase. It has no twinning and ranges in shape from subhedral to anhedral.

The primary accessories are the opaques which are probably mainly magnetite. The grains range from subhedral to anhedral and are mainly equant in shape. Other minor accessory minerals are apatite and sphene

found as small euhedral crystals.

The sections are holocrystalline with phenocrysts set in aphanitic groundmass. The grains show random orientation and distribution (Plate 1). There is no hint of a flow fabric and there is no deformation of the large grains. These observations imply that the rising magma must have been mainly liquid magma with very little, if any, solids or the flow was plug flow, with no shear stresses in the main body of the moving magma (ie. flat velocity profile). There are no skeletal crystals or glass to indicate a rapid cooling. The olivines and augites are commonly equant suggesting a slow growth (equivalent to a slow cooling, perhaps).

Modal percentages were determined by point counting between 1500 and 2000 counts on each thin section. The results (Table 2.1) indicate that the mafic rocks (from the centre of Huerfano Butte) can be classified as an augite-biotite-olivine alkali monzogabbro.

The probable order of crystallization as indicated by textural relationships is apatite and sphene followed by biotite, opaques, olivine, and augite precipitating

Plate 1 Magnification of a thin section in PPL from the gabbroic dyke showing random orientation and distribution of grains. Olivines are easily recognizable due the characteristic curved fractures. Augites are the darker gray grains. The black grains are both opaques and deep red biotite laths. Feldspars make up the light coloured groundmass.

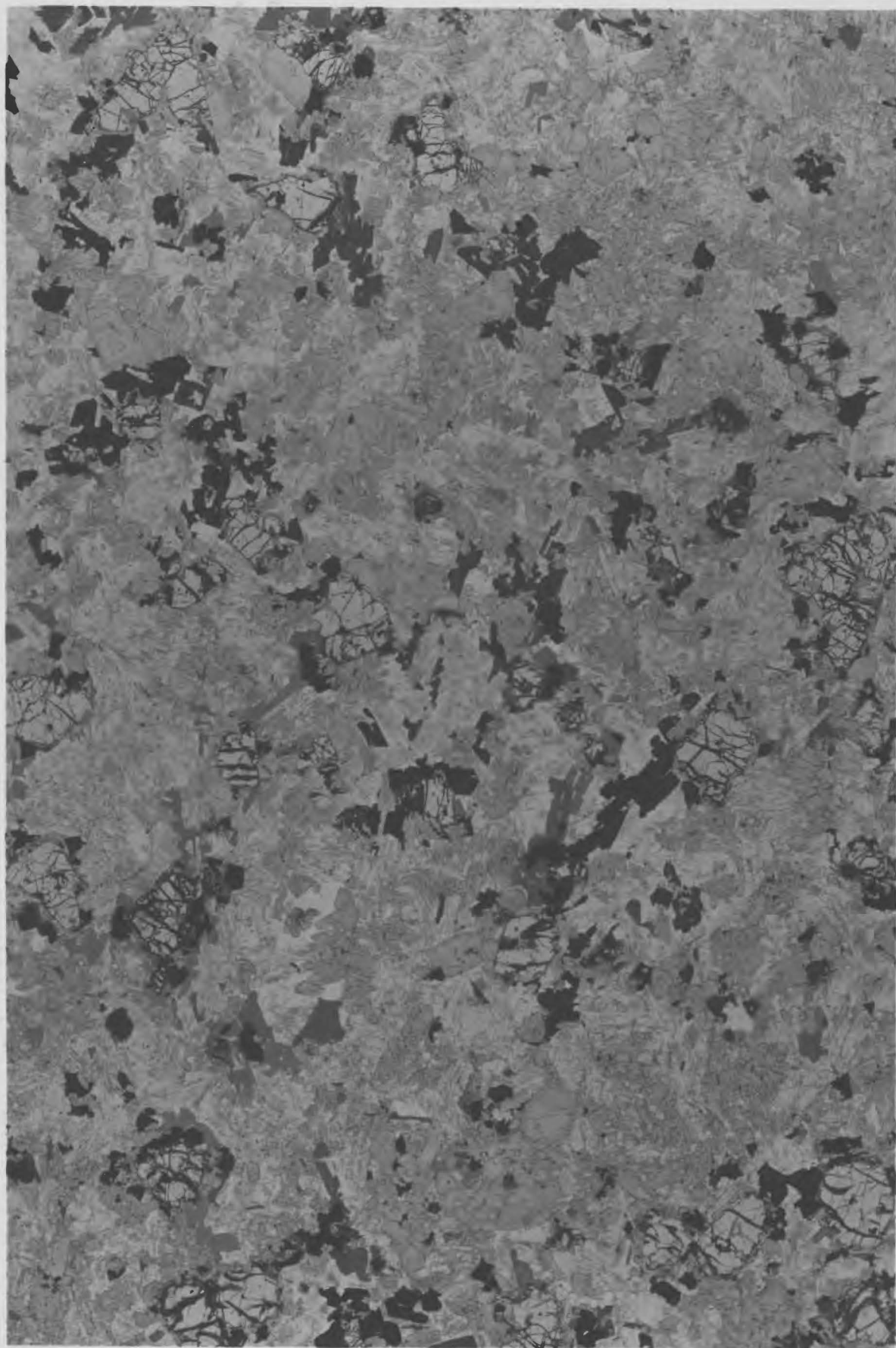


Table 2.1 Mineral Modal percentages for two thin sections from the central dyke and the resulting average.

MINERAL MODAL PERCENTAGES

Mineral Name	#036	#037	Average
plagioclase	29%	30%	29%
augite	29%	27%	28%
biotite	14%	15-16%	15%
olivine	6%	10%	8%
sanidine	11%	11%	11%
opaques	5%	4%	4%
apatite	2%	1%	1%
serpentine	1-2%	1%	1%
analcite	3%	2%	2%
pores	1-2%	-	1%

simultaneously. The last major phases to crystallize were plagioclase and alkali feldspar, followed by the minor alteration of olivine to serpentine and magnetite and alteration of the feldspars to analcite.

3.0 GEOCHEMISTRY

3.1 Introduction

Samples that represent a cross-section of Huerfano Butte to include the central dyke, the outer plug, and the contact between the two have been chemically analyzed.

X-ray fluorescence was used to determine major elements (SiO_2 , Al_2O_3 , MgO , CaO , Na_2O , K_2O , TiO_2 , MnO , and P_2O_5 weight percents) and to determine concentrations of selected trace elements. Rare earth elements and numerous other trace elements were determined by neutron activation techniques.

The results are presented in Tables 3.1, 3.2, 3.3, 3.4, and 3.5 as original oxide data, normalized to 100%, CIPW norms, and trace element concentrations.

3.2 Chemical Trends

The first set of diagrams are the widely used Harker type variation diagrams. There appears to be some controversy about whether trends on these diagrams actually demonstrate fractional crystallization for all

Table 3.1 Major element oxide concentrations as determined by X-ray fluorescence for six samples. Sample numbers 37 and 39 are from the dyke, 34 and 35 are from the dyke/plug contact, and 40 and 41 are from the plug. LOI represents amount of sample lost on ignition.

	#34	#35	#37	#39	#40	#41
SiO ₂	46.63	55.66	48.13	48.39	56.91	59.68
TiO ₂	2.16	1.37	1.78	1.70	1.92	0.54
Al ₂ O ₃	14.72	19.94	12.99	13.58	16.84	19.85
Fe ₂ O ₃	10.98	5.05	11.72	11.49	6.61	2.78
MnO	0.17	0.08	0.16	0.15	0.10	0.04
MgO	5.48	1.45	9.45	9.78	1.50	0.63
CaO	7.01	3.05	9.36	9.51	3.20	1.67
Na ₂ O	4.14	4.79	2.39	2.53	4.48	6.09
K ₂ O	2.76	5.97	1.93	1.94	5.94	6.70
P ₂ O ₅	0.84	0.51	0.65	0.63	0.54	0.20
LOI	5.10	2.15	1.43	0.29	1.97	1.83
TOTAL	99.99	100.02	99.99	99.99	100.01	100.01

Table 3.2 Major element oxides normalized to 100%.

Table 3.3 CIPW norms.

	#34	#35	#37	#39	#40	#41
Ap	1.74	1.10	1.47	1.40	1.20	0.44
Il	0.34	0.17	0.35	0.32	0.22	0.08
Or	15.32	34.44	11.72	11.61	35.57	39.38
Ab	32.90	36.96	20.80	21.68	38.43	40.70
An	12.62	11.52	19.56	20.23	8.41	6.94
Di	7.54	nd	16.15	16.05	nd	nd
Hy	nd	nd	11.63	10.20	2.49	nd
Ol	9.93	3.59	nd	2.72	nd	1.59
Ne	nd	1.42	nd	nd	nd	5.73
C	nd	2.49	nd	nd	nd	0.04
Q	nd	nd	0.76	nd	1.45	nd
Hm	10.34	4.94	12.08	11.67	6.72	2.77
Tn	3.29	nd	4.04	3.81	2.89	nd
Pv	0.87	nd	nd	nd	nd	nd
Ru	nd	1.25	nd	nd	0.65	0.49
TOTAL	94.89	97.87	98.56	99.70	98.04	98.18

**Table 3.4 Trace element concentrations as determined by
X-ray fluorescence.**

ppm	#34	#35	#37	#39	#40	#41
Rb	39.2	99.5	36.0	35.7	109.5	139.3
Sr	613.4	771.7	901.0	884.4	428.7	356.8
Y	27.6	25.7	21.3	20.3	51.4	23.6
Zr	165.3	381.4	153.6	173.0	757.7	505.1
Nb	21.3	79.2	27.4	27.4	206.4	75.7
La	45	44	32	32	94	45
Nd	35	60	27	22	81	55
Ce	63	105	60	53	180	92
Ga	16	16	24	24	16	23
Ba	960	2330	1170	1110	520	165
S%	.10	.01	.12	.01	.01	.01

Table 3.5 Trace element concentrations as determined by
neutron activation.

ppm	#34	#35	#37	#39	#40	#41
Ag	<2	<2	<2	<2	<2	<2
As	<1	1	<1	<1	<1	<1
Au	12	13	11	7	16	5
Ba	1200	3500	1400	1400	660	230
Br	2.3	2.9	2.0	2.4	3.0	2.3
Co	42	17	62	61	21	16
Cr	90	8.7	590	570	11	2.0
Cs	1.9	1.8	1.2	1.3	1.6	3.2
Hf	6.3	11	6.4	6.1	26	13
Mo	2	<2	<2	<2	<2	<2
Ni	<50	<50	170	180	50	<50
Rb	60	140	50	60	150	190
Sb	0.2	0.1	<0.1	0.2	0.2	0.3
Sc	25.2	4.33	34.1	32.7	4.81	0.92
Se	4	10	6	5	23	12
Sr	700	<100	1000	1000	400	400
Ta	1.4	6.7	2.9	3.0	24	5.7
Th	2.8	13	5.0	5.5	14	22
W	43	65	67	83	77	90
Zn	170	50	140	160	80	40
Ir	<5	<5	<5	<5	<5	<5
La	61.5	97.4	55.5	57.6	167	92.4
Ce	123	173	113	118	353	155
Nd	62	55	50	49	137	48
Sm	11.4	10.8	9.66	9.57	23.0	7.20
Eu	1.73	1.70	1.80	2.37	1.94	0.91
Tb	1.3	1.2	1.0	1.0	2.8	0.8
Yb	2.76	4.01	2.48	2.55	6.26	3.72
Lu	0.36	0.58	0.33	0.35	0.72	0.63
U	0.4	3.6	1.6	1.2	3.0	6.7

types of igneous rocks (Bowen 1928, p.117-122, Chayes 1964, fide Carmichael, Turner, Verhoogen 1974) but they are useful in determining enrichment or depletion of elements for a given series of rocks. A possible alternative to such diagrams is suggested by Pearce (1968). These have been examined favourably by Russell and Nicholls (1988). A set of such diagrams reveal that olivine, pyroxene, and plagioclase probably separated together. Plots which should reveal evolutionary control by single mineral differentiation e.g. separation of olivine alone, show no straight line correlation whereas a Pearce element ratio plot of Ca and Na versus Si, all normalized to K, suggests that olivine, pyroxene, and plagioclase simultaneously controlled any differentiation.

Fig. 3.1 shows MgO, Fe₂O₃, and CaO depletion and Fig. 3.2 shows Al₂O₃, Na₂O, and K₂O enrichment as SiO₂ increases.

Nomenclature classification of the samples is according to MacKenzie, Donaldson, and Guilford (1982) in Fig. 3.3. This plot demonstrates a gabbroic to syenitic trend across the Butte from the central dyke to the outer

Fig. 3.1 Harker type variation diagrams showing depletion of CaO, MgO, and Fe₂O₃ with increasing SiO₂.

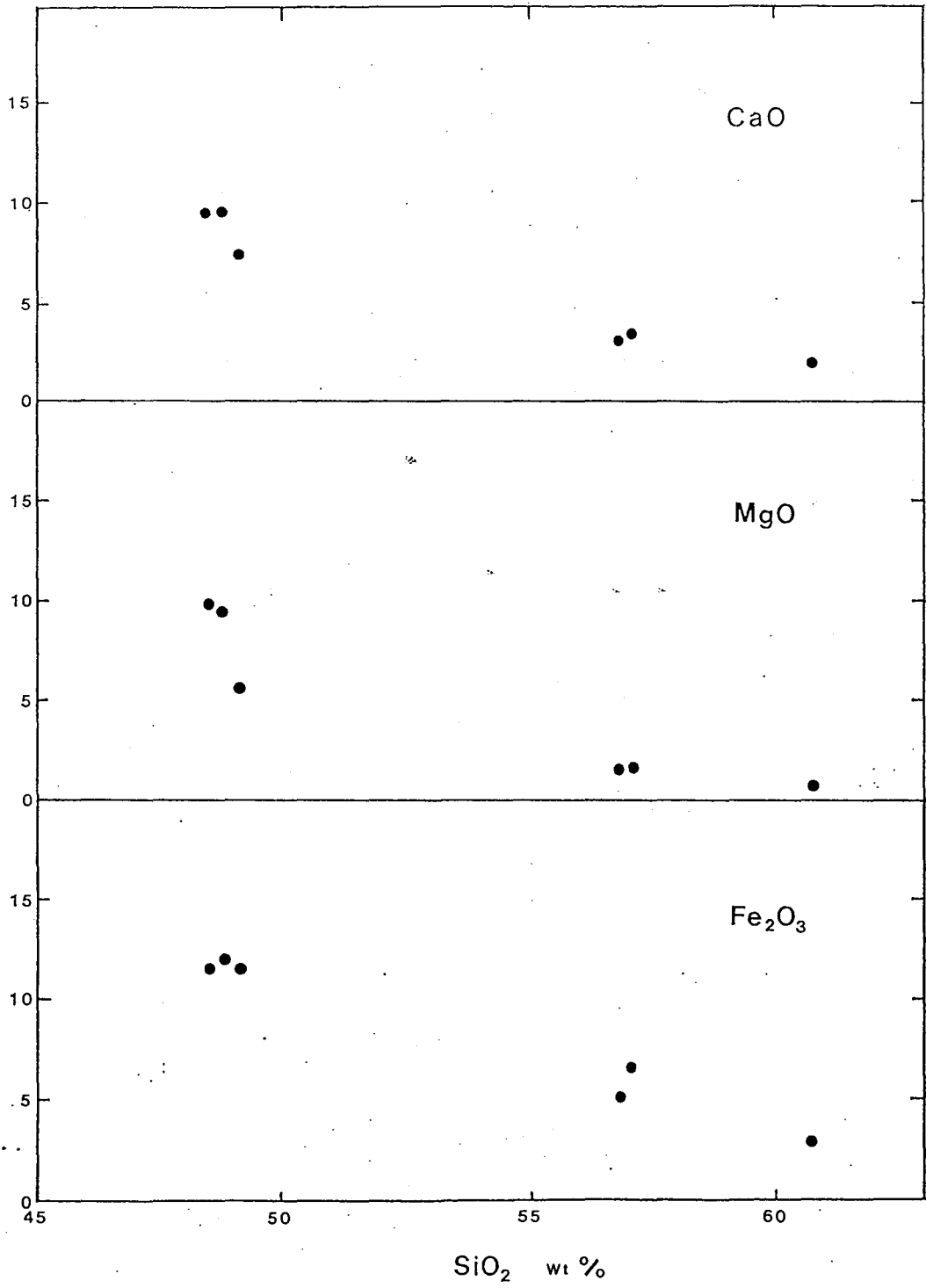
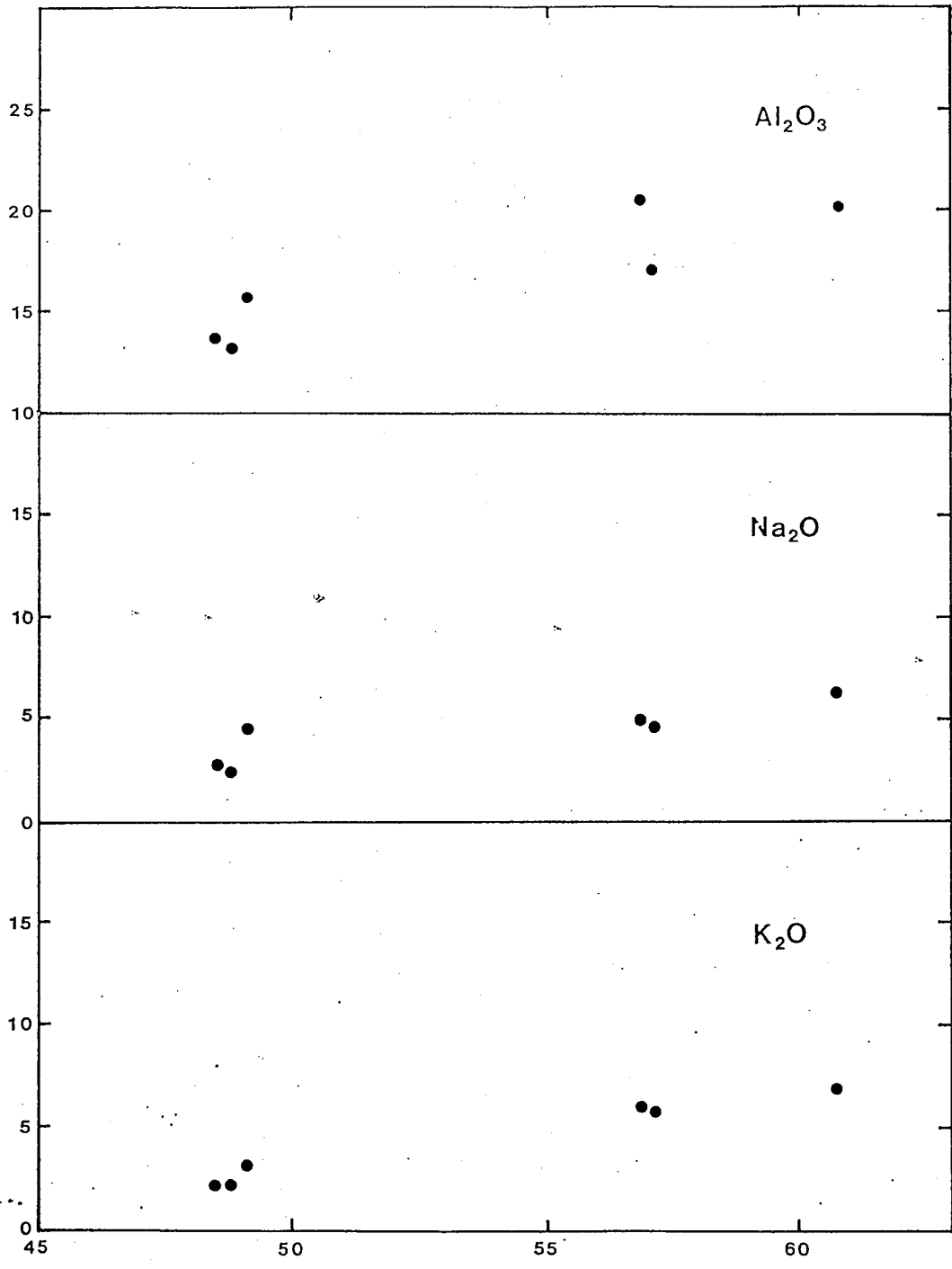
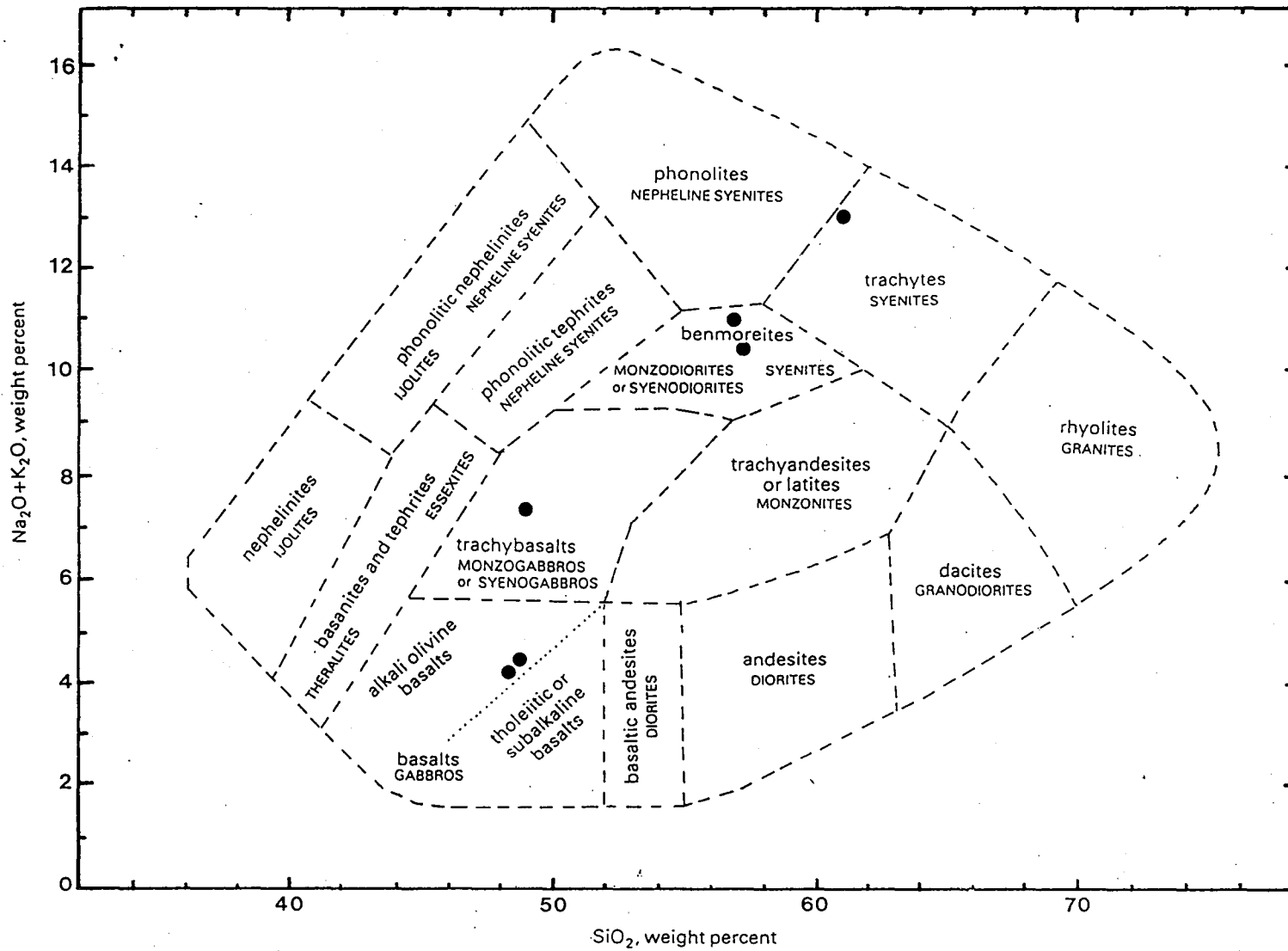


Fig. 3.2 Harker type variation diagrams showing enrichment of Al_2O_3 , Na_2O , and K_2O with increasing SiO_2 .



SiO₂ wt%

Fig. 3.3 Nomenclature classification of the samples.
Coarse grained classes are capitalized and
fine grained classes are non-capitalized.
Modified from MacKenzie, Donaldson, and
Guilford (1982).



plug rim. The MacDonald and Katsura line for defining alkalic versus tholeiitic basalts (gabbros) is also on Fig. 3.3. The data plot on the alkalic portion of the graph. The samples from the central dyke as examined in Chapter 2.0 of this study are classified as an alkali monzogabbro. These samples plot on Fig. 3.3 in the alkali olivine gabbro portion of the graph and thus correspond to the classification determined previously.

An AFM diagram (Fig. 3.4) shows that the dyke samples have higher iron and lower alkali values than the surrounding plug. When compared to other well established basalt trends, the data from this study can be shown to be similar to a fractionated alkali basalt trend though it seems to be slightly lower in iron.

Rare earth analyses of the samples also show differences between the dyke and the plug. Dyke samples are plotted against a chondrite norm in Fig. 3.5 and the plug samples are plotted in Fig. 3.6. All samples show some Eu depletion. The plug samples show a much larger Eu depletion than the dyke implying a higher amount of fractionation of some mineral phase that is Eu compatible (possibly plagioclase) in the plug magma than the dyke

Fig. 3.4 AFM diagram showing various basaltic trends for comparison; dots - this study, solid line - Skaergard pluton Fe rich tholeiite basalt trend (Carmichael, Turner, and Verhoogen, 1974), hatchured line - alkali basalt trend including St. Helena, New South Wales, New Zealand (Smith, 1979), dashed line - Cascades calc alkaline basalt trend (Smith, 1979).

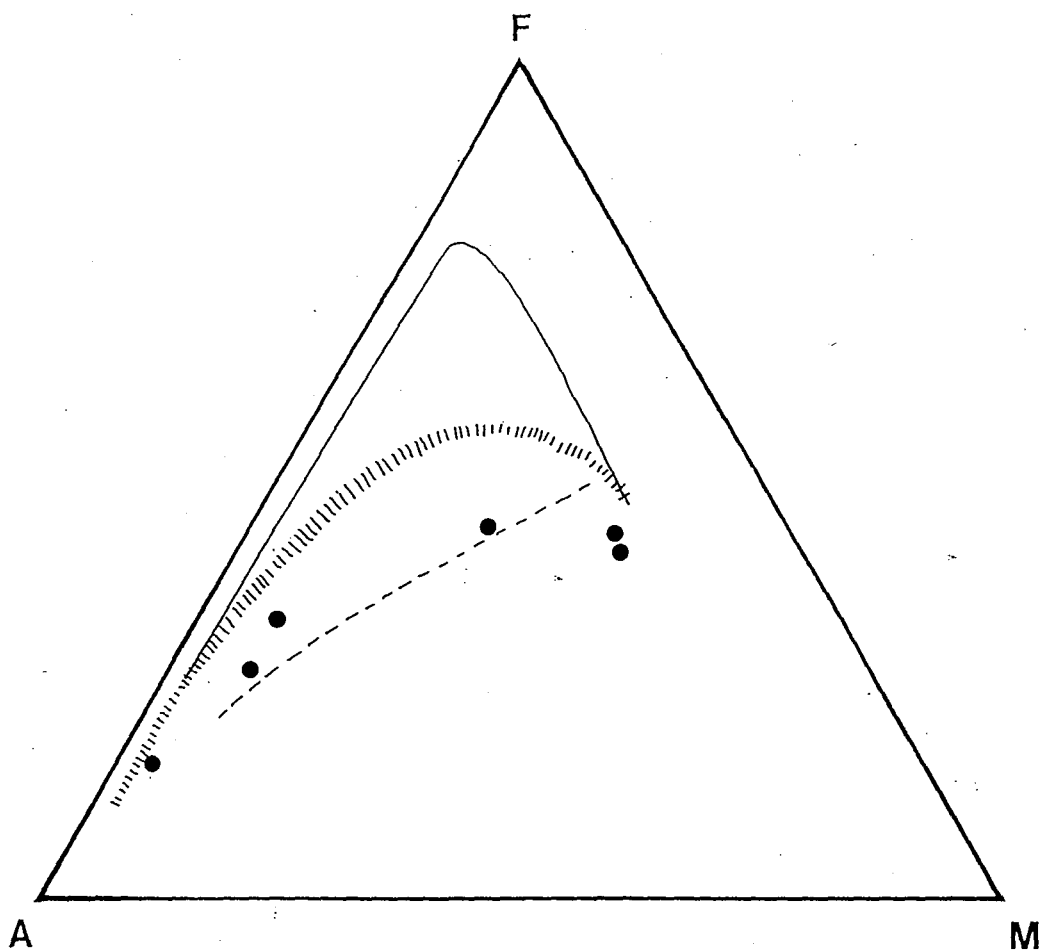


Fig. 3.5 Rare earth elements versus chondrite normalized for the gabbroic dyke. The plot shows a negative Eu anomaly and depletion of heavy rare earth elements over light rare earth elements.

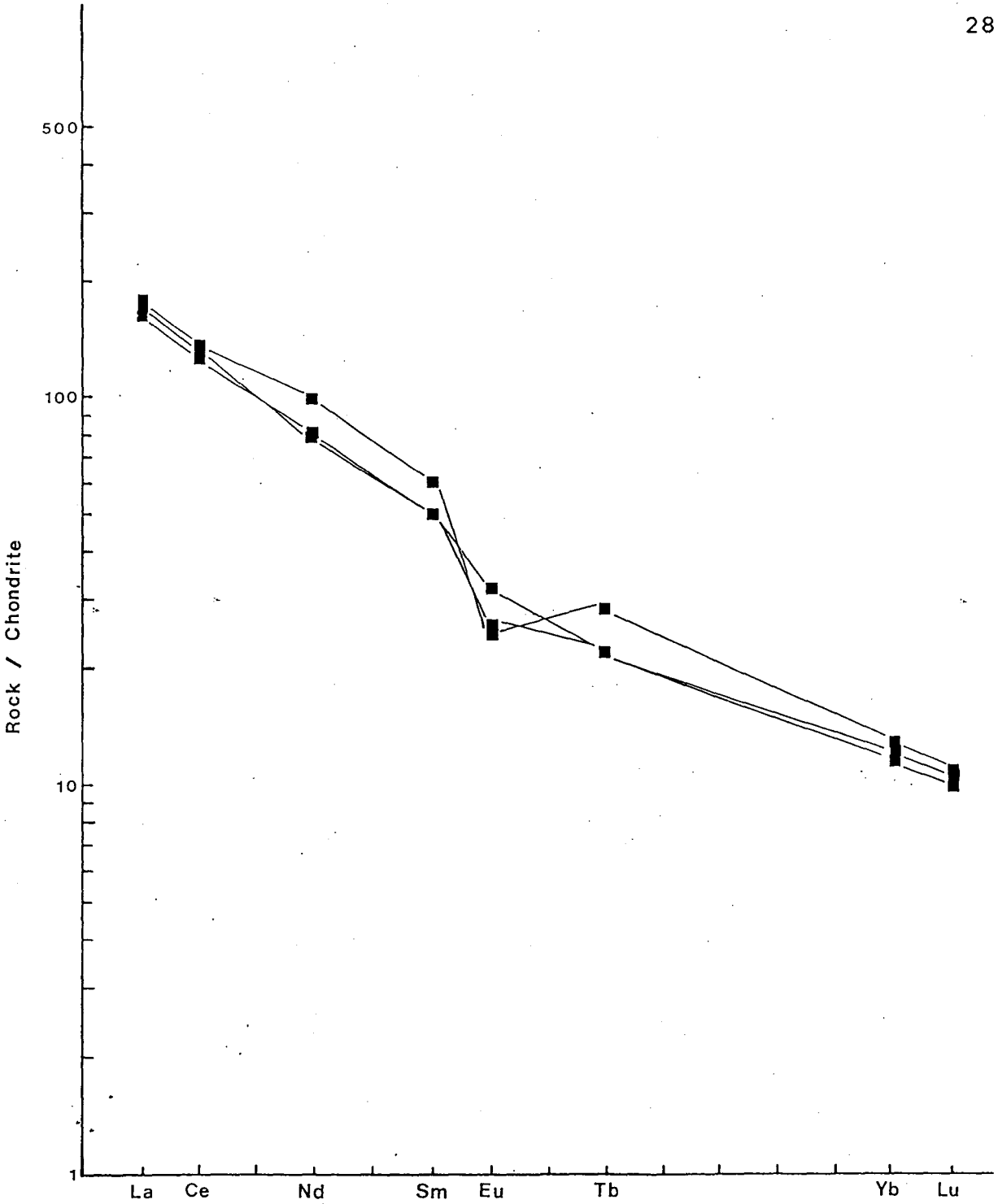
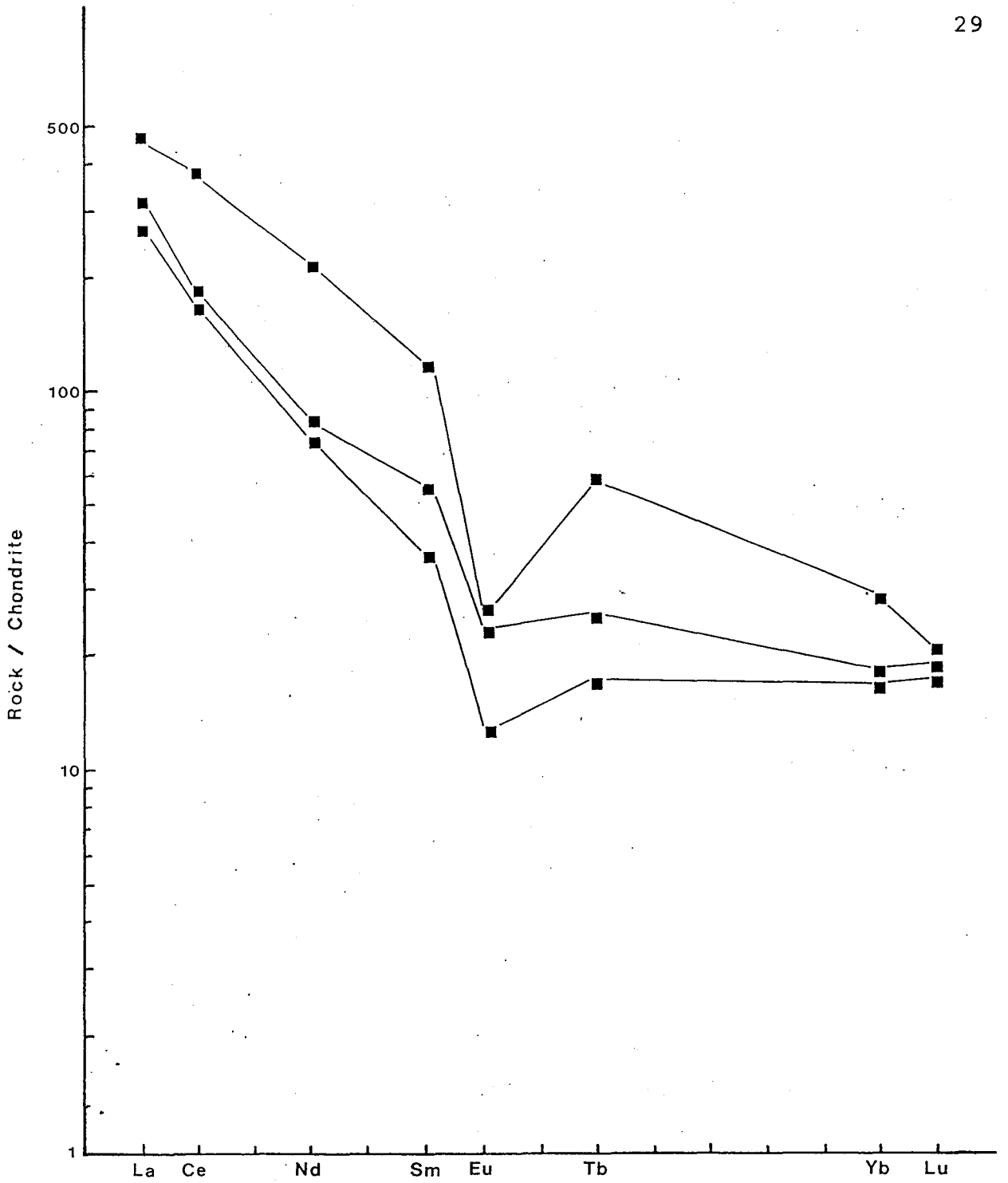


Fig. 3.6 Rare earth elements versus chondrite normalized for the syenitic plug. The plot shows a larger negative Eu anomaly and greater depletion of heavy rare earth elements over light rare earth elements.



magma. The concentrations of the incompatible elements in the plug syenites are approximately double that of the dyke gabbros. This also implies that there is higher fractionation of the plug magma such that incompatible element concentrations have increased over the dyke magma. The slopes of both curves imply that at least some fractionation has occurred in that there is much less heavy rare earths present than light rare earth elements.

3.3 Interpretation

All of the chemical variation diagrams shown define a trend of fractionation from a gabbroic dyke to a syenitic plug. Normally this would result in the placement of the dyke followed by the plug. However, field relationships show that the plug intruded before the dyke. There are two possible explanations to get this apparent reverse fractionation. One explanation could be that there are two different source magmas; a high fractionated source for the plug and a less fractionated source for the dyke with the dyke intruding after the placement of the plug. The other explanation could be that there is only one source; a magma chamber

with an upper highly fractionated level and a lower less fractionated level. If magma is extruded from the chamber over time and there is no new supply of magma added to the chamber, then the magma level will gradually drop. Therefore, the plug could be derived from the upper (high fractionated) level and then later intruded by a pulse of lower level (less fractionated) magma that has become accessible due to the lowering of the magma level in the chamber over time.

3.4 Comparisons

It seems likely that Huerfano Butte is associated with Rio Grande rifting activity. They are both approximately the same age and the alkali composition of the Butte matches the generally alkalic trend of the flanks of the Rift (BVSP, 1981, p.108-131).

One of the largest volcanic fields in the Rio Grande Rift makes up the Taos Plateau. It is a classic suite of silicic, alkali-rich Rio Grande Rift lavas. The Taos volcanics are comparable to Huerfano Butte in major element oxides and in CIPW normatives such as olivine. Comparison of some trace elements such as Nb and Zr show a good correlation between Huerfano Butte and certain

alkali basalts of Taos Plateau (Fig. 3.7). Rare earth element diagrams (Fig. 3.8) show that the Taos volcanics have similar slopes to Huerfano Butte though the Taos concentrations are lower.

Comparison of Huerfano Butte to the Spanish Peaks Dyke complex of alkali and lime oxides versus SiO_2 , shows little agreement (Fig. 3.9). Huerfano Butte has a much wider range in values than the Spanish Peaks. There is better agreement with AFM diagrams in that Spanish Peaks covers a wide range that includes the Huerfano Butte trend.

Thus, it would seem that the conditions that prevailed in the making of the Taos Plateau may be rather similar to that of Huerfano Butte. Though Huerfano Butte is similar in age and close to the location of the Spanish Peaks complex, the conditions that formed the complex were probably different from those that formed the alkali basalt fractionation trend of Huerfano Butte.

Fig. 3.7 Comparison of Huerfano Butte to Taos Plateau compositions for lines of constant ratio for Nb and Zr. Nephelinites fall around the 2.6 line; alkali basalts approximately 5.5 to 7.5; Servilleta tholeiites about 12.0; dots - Huerfano Butte. (Modified from BVSP, 1981)

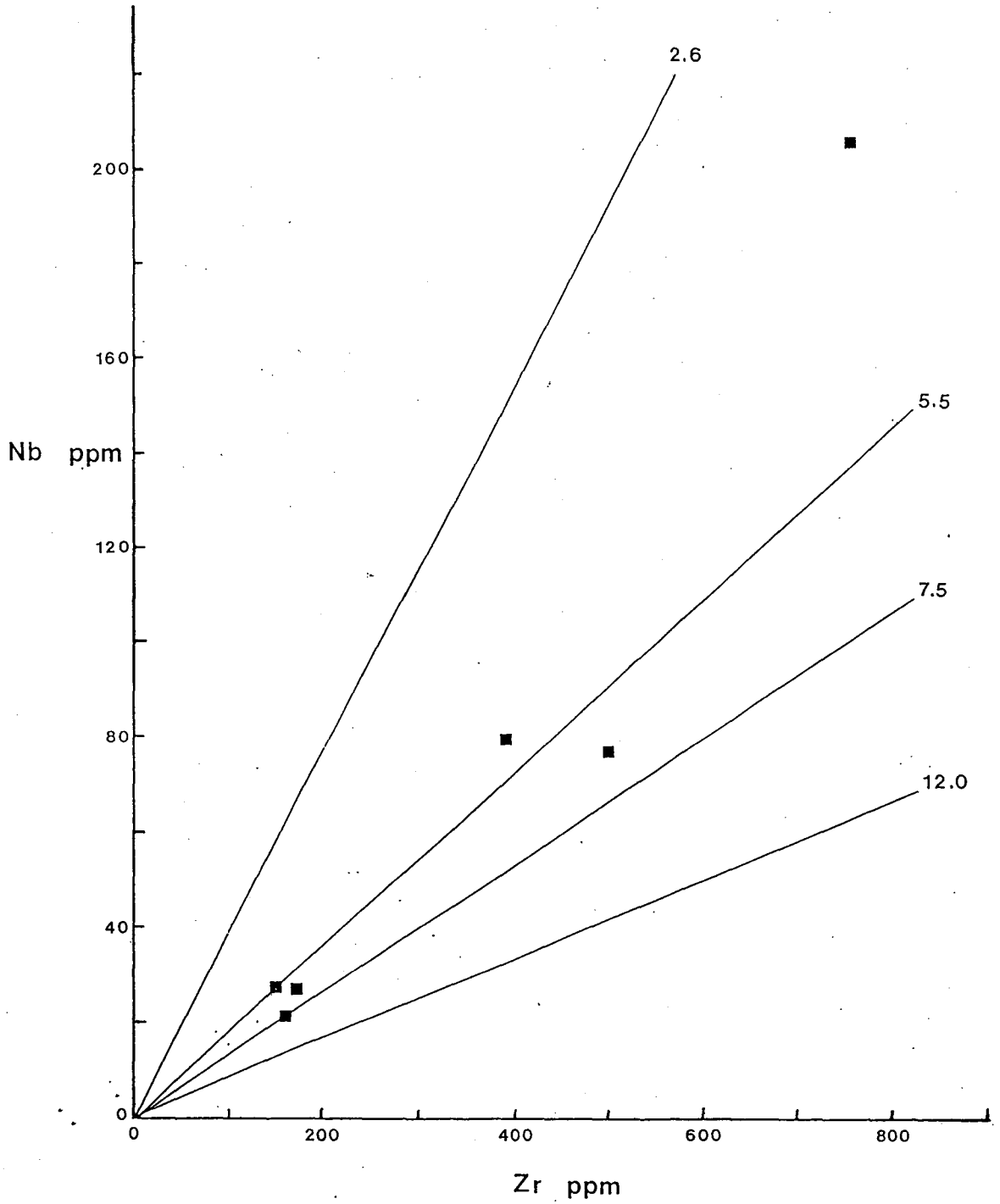


Fig. 3.8 Rare earth element diagram comparing
Huerfano Butte to Taos Plateau trends
(modified from BSVP, 1981).

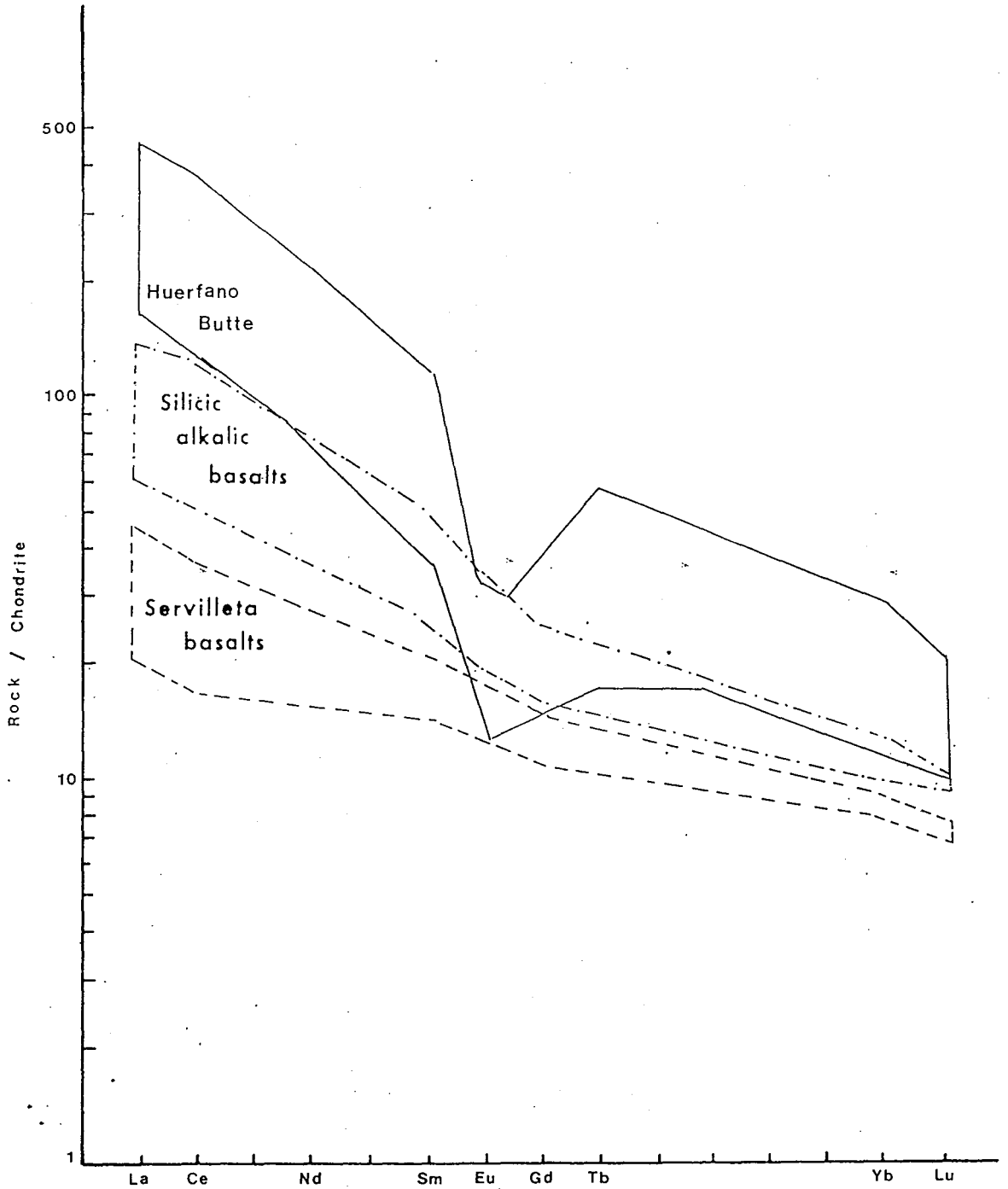
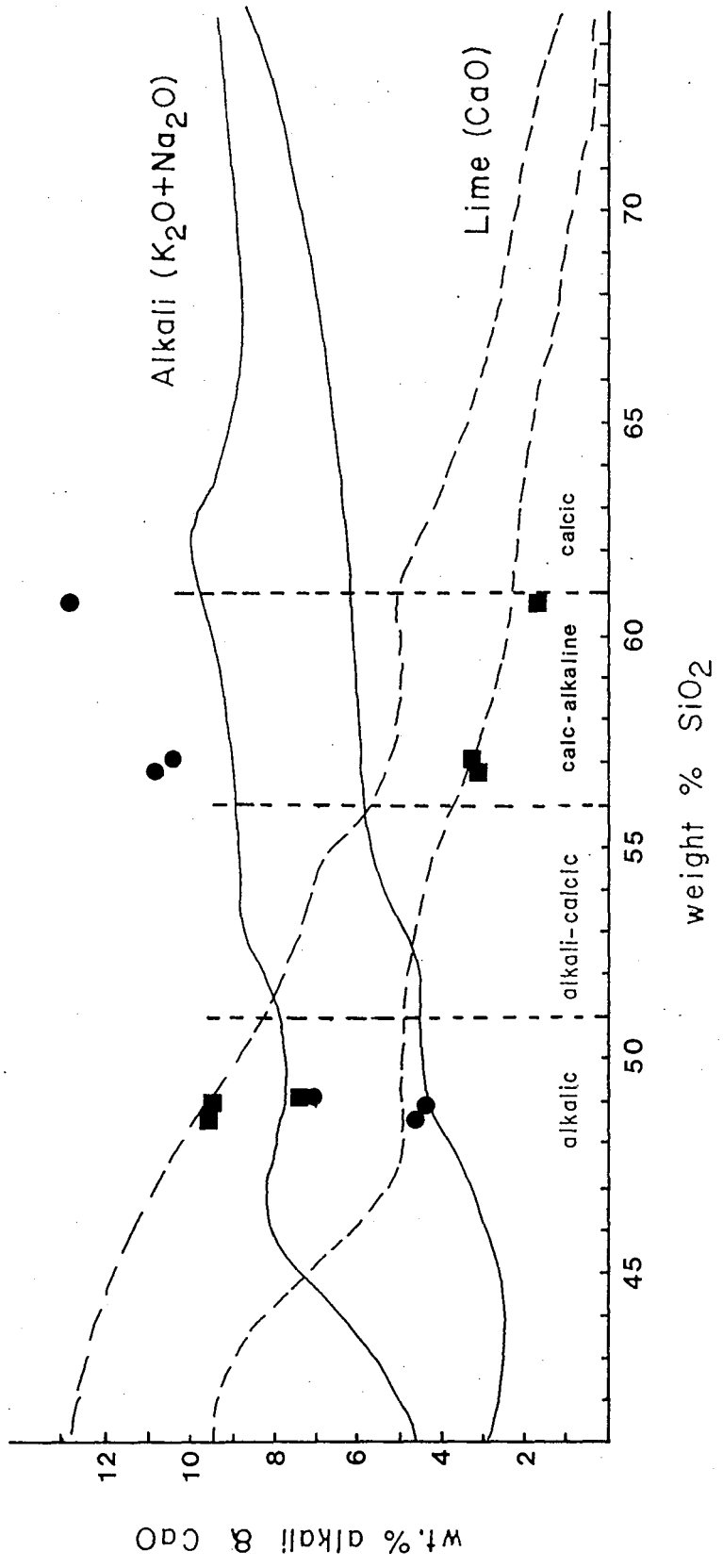


Fig. 3.9 Alkali and lime trends for the Spanish Peaks Dyke Complex. Dots and squares show Huerfano Butte alkali trend and lime trend respectively (modified from Smith 1979).



4.0 CRYSTAL SIZE DISTRIBUTION THEORY

4.1 Introduction

The question of magmatic crystallization is one of long standing. The use of terms like "porphyritic", "phenocryst" and "groundmass" are typical examples of the importance in interpretations of what we think we see in rocks.

Attempts to link grain size variation with nucleation and genetic processes have been made by Winkler (1949), Gray (1970) and Kirkpatrick (1975). More recently, Marsh and others have examined grain size characteristics of igneous rocks in a rather different fashion. Marsh (1981), after examining a great many volcanic rocks concluded that there is a connection between the volume abundance of phenocrysts in a magma and the probability that this magma will appear as a lava flow, specifically that there is an upper bound on phenocryst content if a magma is to emerge at the earth's surface, and that this upper bound is likely to vary inversely as viscosity which varies with silica content. It follows that nucleation and growth rates are important, especially in relation to cooling rates, in

the physical evolution of magma/lavas. Marsh (1988), Cashman (1988) and Cashman and Marsh (1988) provide insight into these ratios, in a very simple way, namely, using crystal size distribution.

4.2 Outline of CSD Theory

The basic premise of CSD is that crystal size is perhaps the most characteristic feature of igneous and metamorphic rocks. Since "rocks are often quenched during nucleation and growth, the numbers of crystals per size range can reflect the kinetics of crystallization" (Marsh 1988, p.277). Hence, construction of semilogarithmic plots of numbers of crystals per size versus size should yield information on nucleation and growth rates.

4.3 Methodology of CSD Analysis

The methodology of CSD requires that first, the population density is found as a function of the number of crystals per size versus size using the equation

$$n(L) = \frac{dN(L)}{dL} \quad (1)$$

or

$$n(L) = \frac{\Delta N(L)}{\Delta L} \quad (2)$$

Equation (1) includes a volume correction useful for inequant grain shapes. Since the grains in this study were commonly equant shaped, the simpler equation (2) is used. Then the appropriate crystal population balance equation is found

$$(V_2 n_2 - V_1 n_1) \Delta L = (G_1 V_1 n_1 - G_2 V_2 n_2) \Delta t + (Q_i n_i - Q_o n_o) \Delta t \Delta L \quad (3)$$

(net accumulation) = (growth input - growth output)
+ (flux in - flux out)

Manipulation of equation (3) by dividing by $\Delta t \Delta L$ and letting both approach zero gives

$$\frac{\partial (Vn)}{\partial t} + \frac{\partial (GVn)}{\partial L} = Q_i n_i - Q_o n_o \quad (4)$$

Solving equation (4) depends on the type of igneous body that is being analyzed. For the Huerfano Butte dyke, assume that there is no inflow or outflow of magma once the flow is in place. This leads to the implication that the amount of magma available for crystallization decreases with time. One last necessary assumption for solving the equation is that growth rate G is constant. Without this assumption the equation becomes very difficult to solve. Equation (4) can now be reduced to

$$\frac{\partial (Vn)}{\partial t} + G \frac{\partial (Vn)}{\partial L} = 0 \quad (5)$$

The general solution for equation (5) can be found for a non steady state (no inflow or outflow)

$$n = \left(\frac{V_0}{V(t)} \right) n^0 \exp \left[- \frac{L}{hG} + \frac{t}{h} \right] \quad (6)$$

where n^0 is the nucleii population density and is found as the intercept at $L=0$ and $-1/Gh$ is the slope of the plot and gives growth rate. These equations show that much of the numerical information can be found directly from semilogarithmic plots of number of crystals per size $N(L)$ versus size L and that these numbers as well as the shape of the plot will give information on the history of the igneous body.

Effective residence time, T (or h , specifically for non steady state flow), must be found independently of the graph. An estimate of 50 years (1.5×10^9 seconds) was chosen as a maximum value for nucleation time given that Huerfano Butte is comparable in size to lava pools in Hawaii with known overall crystallizing times of 20 to 50 years. The maximum limit of 50 years was chosen since it is believed that the current level of Huerfano Butte was perhaps one kilometer below the surface at the time of intrusion. It was therefore insulated much more than any Hawaiian lava pools, and so cooled slower. There is much evidence of wide spread erosion throughout the region and one kilometer is a rough mid-range value for

the thickness of stratigraphic units which probably covered the area (Johnson, 1959). Other estimates of T are about 10^5 to 10^6 seconds for extrusive magmatic facies and 10^8 seconds in intrusive regions (Brandeis and Jaupart, 1987). Clearly the 50 year value assigned to T is high by an order of magnitude relative to the upper value of Brandeis and Jaupart. The imprecision of this value is not critical in CSD theory for the nucleation rate, which is rather insensitive to variations in T ; growth rate varies inversely with T , however, so inferences of growth rate here are definitely low.

Two thin sections from Huerfano Butte were used for the analysis. Inspection of these sections showed that there is no preferred orientation or distribution of any of the mineral phases and thus there should be no size bias due to orientation or abundance variations because of inhomogeneities in distribution at the scale of the thin section.

The phases chosen for CSD were magnetite and olivine as two of the earliest forming phases and therefore least likely to have had any interference in nucleation and growth by any succeeding phases. Images of the thin sections were projected onto a screen in plane light. The maximum dimension for each grain of magnetite was

measured using a straight edge consistently readable to 0.125 inch on the screen. This is about the limit of clear recognition of grain boundaries and corresponds to 0.04 mm in absolute size (Table 4.1). A microscope with a graded eyepiece was used to obtain the maximum dimension for each crystal of olivine using both 40 power and 100 power magnification (Table 4.2).

4.4 Results

Corresponding graphs of CSD, expressed as natural logarithms of population density size versus (linear) size are shown as Fig. 4.1 and 4.2.

From the magnetite plots, we can see that within small limits the trend is linear in this frame. The best fit lines have been established by linear regression. Coefficients of regression are approximately 0.97. The fitted line has been extended to the left to define the intercept value of $\ln(n)$ at $L=0$. The slope of the curve is $-1/GT$ where G is growth rate (cm/s) and T is effective residence time.

From the olivine plots, we see that there is not a simple linear trend but a curve that can be broken into two parts; one convex upward curved trend for small L and

Table 4.1 Results of measuring maximum dimensions
of magnetite grains for two samples.

LENGTH (cm)	#36	#37
0.000 - 0.0039	251	220
0.004 - 0.0079	235	216
0.008 - 0.0119	211	169
0.012 - 0.0159	167	153
0.016 - 0.0199	115	106
0.020 - 0.0239	68	47
0.024 - 0.0279	21	27
0.028 - 0.0319	16	17
0.032 - 0.0359	7	2
0.036 - 0.0399	5	3
Total # grains	1096	960

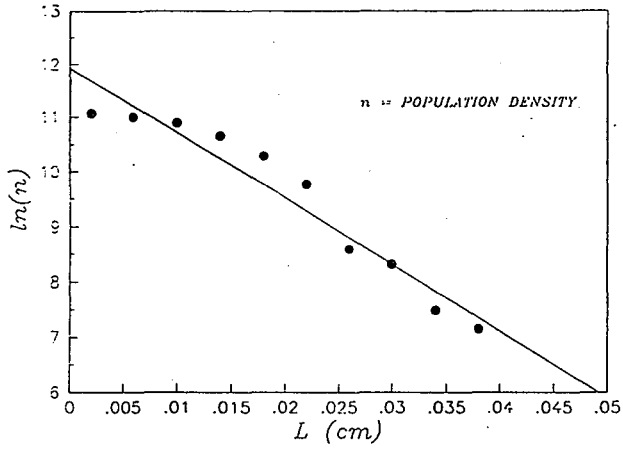
Table 4.2 Results of measuring maximum dimensions
of olivine grains for one sample.

LENGTH (cm)	#37
0.000 - 0.0049	1
0.005 - 0.0099	6
0.010 - 0.0149	16
0.015 - 0.0199	22
0.020 - 0.0249	28
0.025 - 0.0299	24
0.030 - 0.0349	30
0.035 - 0.0399	29
0.040 - 0.0449	33
0.045 - 0.0499	21
0.050 - 0.0549	19
0.055 - 0.0599	10
0.060 - 0.0649	20
0.065 - 0.0699	11
0.070 - 0.0749	10
0.075 - 0.0799	10
0.080 - 0.0849	9
0.085 - 0.0899	13
0.090 - 0.0949	6
0.095 - 0.0999	8
0.100 - 0.1049	5
0.105 - 0.1099	1
0.110 - 0.1149	2
0.115 - 0.1199	5
0.120 - 0.1249	1
0.125 - 0.1299	2
0.130 - 0.1349	1
0.135 - 0.1399	1
Total # grains	344

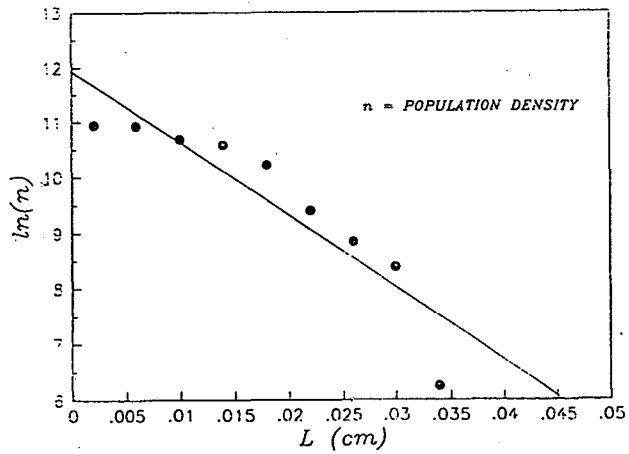
Fig. 4.1 Population density versus length for opaque grains obtained by modifying Table 4.1 by Equation (2). Linear least squares regression provided a best fit line for obtaining the $L=0$ intercept (n° nucleation density).

Fig. 4.2 Population density versus length for olivine grains obtained by modifying Table 4.2 by Equation (2). The data does not fit a simple linear trend.

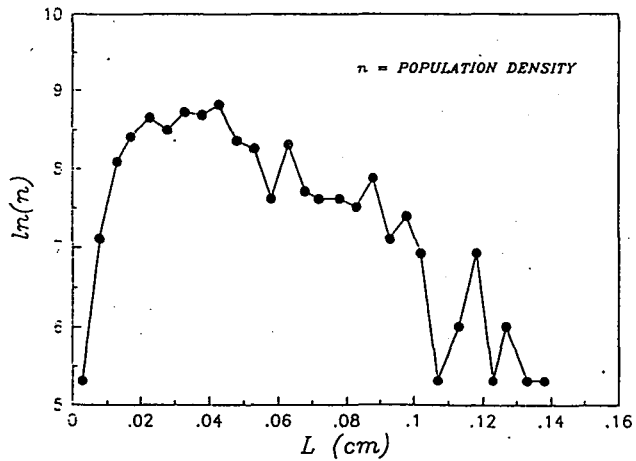
OPAQUES - #036



OPAQUES - #037



OLIVINES - #37



another linear trend for large L. The portion of the curve for small L has a slope of $+1/GT$; therefore growth rate G must have been negative. The implications of this are discussed below. The linear portion for large L will have a slope of $-1/GT$ where growth rate G must be positive.

4.5 Interpretations

The straight line plots for magnetite have several implications.

- i) growth and nucleation were continuous throughout the residence time,
- ii) crystal growth occurred without size dependent crystal growth,
- iii) crystallization occurred without significant fractionation within the crystallizing volume.

Slight differences in values obtained by this study as compared to the values obtained by Cashman and Marsh (1988) (Table 4.3) can be attributed to the differences between their study samples and these from Huerfano Butte. The samples used by Cashman and Marsh, from Makaopuhi lava lake, ranged from 20% to 80% crystals in

Table 4.3 CSD values for opaques from Huerfano Butte and Makaopuhi lava lake. T is effective residence time; slope ($1/GT$) is obtained from linear regression; G (growth rate) is slope/T; n° (nucleation density) is the intercept at $L=0$; J (nucleation rate) is $n^{\circ} \times G$.

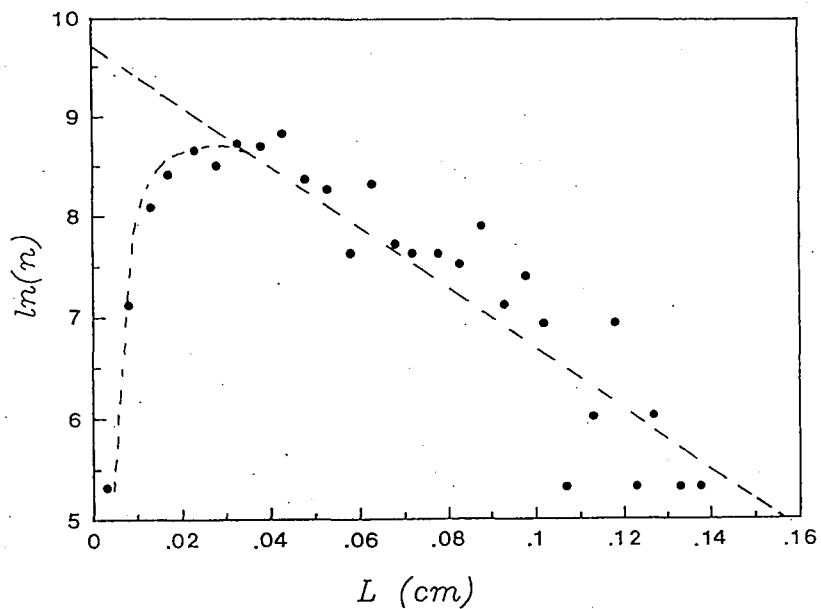
	T sec	slope cm^{-1}	G cm/s	$n^{\circ} \text{cm}^{-4}$	J $\text{cm}^{-3} \text{s}^{-1}$
#36	1.5×10^9	-120	8.0×10^{-8}	1.52×10^5	1.2×10^{-2}
#37	1.5×10^9	-135	9.0×10^{-8}	1.59×10^5	1.4×10^{-2}
C & M	6.25×10^6	-555	2.7×10^{-10}	2.07×10^6	7.6×10^{-2}

the groundmass. They showed that the slopes of the plots decreased with increasing crystallinity. Also the iron oxide plots for the Makaopuhi lava lake samples are for a combination of magnetite and ilmenite since they were not treated separately by Cashman and Marsh.

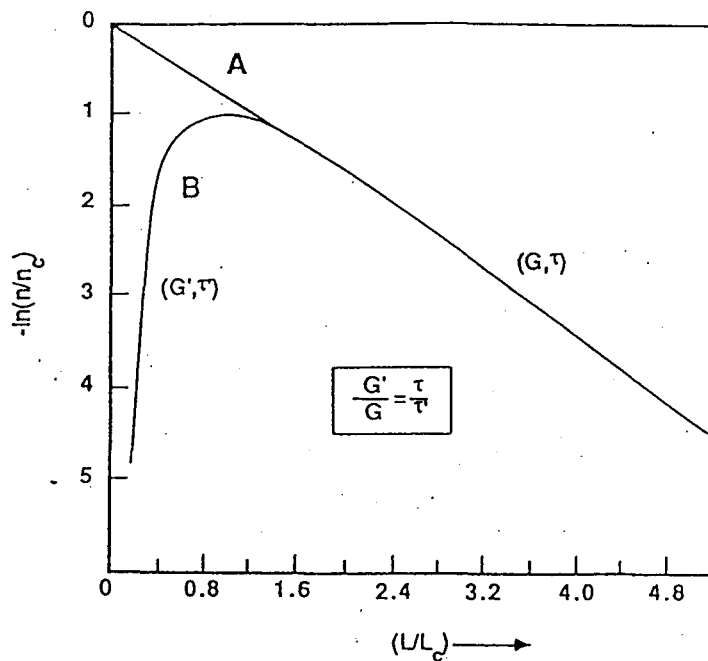
The curve of the olivine plot is not a simple straight line. It suggests that there were two rates of growth. Where grain size L is small and the curve has a positive slope, G must be negative (since T must be positive). Thus G is not so much a growth rate as an effective resorption rate with an effective mean resorption time, $T_r \leq T$. Where L is large, G is a real and positive growth rate and T is residence time for the entire history of crystallization. The two portions of the curve thus imply that small olivine crystals perhaps below some critical size L_c have undergone resorption, decreasing in size and numbers with the resorbed material perhaps being absorbed into the larger crystals and thus increasing the size of grains above L_c (Fig. 4.4). The effect will be to change the slope of the straight line portion of the graph for the higher values of L , and perhaps to extend it to even higher values of L ; and to alter the slope of the curve for the lower values of L .

Fig. 4.3 Comparison of olivine CSD plot from Huerfano Butte to Marsh (1988) theoretical curve due to annealing of small grains.

OLIVINES - #37



THEORETICAL



There is no sign of zoning in the large grains under a microscope with polarized light; perhaps some other procedure may find evidence of zoning. Taking absence of zoning at face value, it implies no change in the composition of the magma of a kind to demand zoning of the olivines.

4.6 Error Discussion

No formal estimation of errors has been made for this study. Clearly the cut effect in a thin section leads to errors in the estimate of average real size. Further the grains are not spheres but irregular polyhedra.

Translation of size data from random sections through such bodies into "real" dimensions is not possible with any high degree of accuracy or precision. A brief review of the problems involved is given in an appendix in Cashman and Marsh (1988). Here, it suffices to note that measured values give information relative to other samples in the same study. Cashman (1988) suggests that the numerical values acquired are low by 5-15% in absolute terms.

4.7 Conclusions

The values for J and G for magnetite found for Huerfano Butte are comparable with data from Makaopuhi lava lake (Cashman and Marsh 1988); following these authors, their conclusions should hold for Huerfano Butte. The implications of the straight lines are that crystal nucleation and growth were continuous over time T, that there was no dependency of crystal growth rate or crystal size, and that there has been no significant crystal fractionation in our specimens.

Increasing crystallinity lowers G and J up to one order of magnitude as seen when comparing values of Huerfano Butte to Makaopuhi lava lake.

There is the further implication that undercooling T to which J is closely linked, was relatively small (Cashman and Marsh, 1988 p.301) else nucleation rates would be larger.

The continuity of the curves accords with data from other studies (Cashman 1988, Cashman and Marsh 1988) and suggest that the notion of phenocrysts with its implication of grain size bimodality should be treated with reserve.

BIBLIOGRAPHY

- BSVP (1981) Basaltic Volcanism on the Terrestrial Planets, Pergamon Press, pp.1286
- Bowen, N.L. (1928) The Evolution of the Igneous Rocks, Princeton University Press, Princeton, New Jersey
- Brandeis, G., Jaupart, C. (1987) The kinetics of nucleation and crystal growth and scaling laws for magmatic crystallization. Cont. Mineral. Petrol. 96:24-34
- Carmichael, I., Turner, J.T., Verhoogen, J. (1974) Igneous Petrology, McGraw-Hill Inc. pp.739
- Cashman, K.V. (1988) Crystallization of Mount St. Helens 1980-1986 Dacite: A quantitative textural approach. Bull. Volcanology 50:194-209
- _____, Marsh, B.D. (1988) Crystal Size Distribution (CSD) in rocks and the kinetics and dynamics of crystallization II: Makaopuhi lava lake. Cont. Mineral. Petrol. 99:292-305
- Chapin, C.E. (1979) Evolution of the Rio Grande Rift - A Summary in Rio Grande Rift: Tectonics and Magmatism (ed. Riecker) p.1-5
- Chayes, F. (1964) Variance - covariance relations in some published Harker diagrams of volcanic suites. J. Petrol. 5:219-237
- Eaton, G.P. (1979) A plate tectonic model for Late Cenozoic crustal spreading in the Western United States in Rio Grande Rift: Tectonism and Magmatism (ed. Riecker) p.7-32
- Johnson, R.B. (1959) Geology of the Huerfano Park area Huerfano and Custer Counties Colorado. G.S.A. Bull. 1071-D
- _____, (1968) Geology of the igneous rocks of the Spanish Peaks region Colorado. G.S.A. Prof. Paper 594-G

- _____ (1970) Patterns and origins of radial dyke swarms associated with West Spanish Peak and Dyke Mountain, South - Central Colorado. G.S.A. Bull. 72:579-590
- Kirkpatrick, R.J. (1975) Crystal growth from a melt - A review. Am. Mineral. 60:798-814
- Knopf, A. (1936) Igneous geology of the Spanish Peaks region Colorado. G.S.A. Bull. 47:1727-1784
- MacDonald, G.A., Katsura, T. (1964) Chemical composition of Hawaiian lavas. J. Petrol. 5:82-133
- MacKenzie, W.S., Donaldson, C.H., Guilford, C. (1982) Atlas of Igneous Rocks and their Textures, Halstead Press, New York, pp.148
- Marvin, R.F., Young, E.J., Mehnert, H.H., Naeser, C.W. (1974) Summary of radiometric age determinations of Mesozoic and Cenozoic igneous rocks and uranium and base metals deposits in Colorado. Isochron/West 11
- Marsh, B.D. (1981) On the crystallinity, probability of occurrence and rheology of lava and magma. Cont. Mineral. Petrol. 78:85-98
- _____ (1988) Crystal Size Distribution (CSD) in rocks and the kinetics and dynamics of crystallization. Cont. Mineral. Petrol. 99:277-291
- Nockolds, S.R., Knox, R.W., Chinner, G.A. (1978) Petrology for Students, Cambridge University Press, pp.435
- Pearce, T.H. (1968) A contribution to the theory of variation diagrams. Cont. Mineral. Petrol. 19:142-157
- Philpotts, A.R. (1988) Petrography of Igneous and Metamorphic Rocks, Prentice Hall, New Jersey
- Richardson, S.M., McSween Jr., H.Y. (1989) Geochemistry, Pathways and Processes, Prentice Hall, New Jersey, pp.488
- Russell, J.K. Nicholls, J. (1988) Analysis of petrographic hypotheses with Pearce Element Ratios. Cont. Mineral. Petrol. 99:25-35

- Smith, R.P. (1979) Early rift magmatism at Spanish Peaks, Colorado in Rio Grande Rift: Tectonism and Magmatism (ed. Riecker) p.313-321
- Stormer, J.C. (1972) Ages and nature of volcanic activity on the southern High Plains, New Mexico and Colorado. G.S.A. Bull. 83:2443-2448
- Tweto, O. (1979) The Rio Grande Rift system in Colorado in Rio Grande Rift: Tectonism and Magmatism (ed. Riecker) p.33-56
- _____ (1980a) Tectonic history of Colorado in Colorado Geology, RMAG, Denver Colorado, p.5-10
- _____ (1980b) Precambrian Geology of Colorado, RMAG, Denver Colorado, p.37-46
- _____ (1980c) Summary of Laramide orogeny in Colorado in Colorado, RMAG, Denver Colorado, p.129-134
- Williams, H., Turner, F.J., Gilbert, C.M. (1982) Petrography, An Introduction to the Study of Rocks in Thin Sections, W.H. Freeman and Company, San Francisco, pp.626
- Winkler, H.G.F. (1949) Crystallization of basaltic magma as recorded by variation of crystal-size in dykes. Mineral. Mag. 28:557-574